How stationary are the internal tides in a high-resolution global ocean circulation model?

Jay F. Shriver[1], James G. Richman[1], and Brian K. Arbic[2]

[1]Oceanography Division, Naval Research Laboratory, Stennis Space Center, Mississippi, USA, [2]Department of Earth and Environmental Sciences, University of Michigan, Ann Arbor, Michigan, USA

Abstract The stationarity of the internal tides generated in a global eddy-resolving ocean circulation model forced by realistic atmospheric fluxes and the luni-solar gravitational potential is explored. The root mean square (RMS) variability in the M_2 internal tidal amplitude is approximately 2 mm or less over most of the ocean and exceeds 2 mm in regions with larger internal tidal amplitude. The M_2 RMS variability approaches the mean amplitude in weaker tidal areas such as the tropical Pacific and eastern Indian Ocean, but is smaller than the mean amplitude near generation regions. Approximately 60% of the variance in the complex M_2 tidal amplitude is due to amplitude-weighted phase variations. Using the RMS tidal amplitude variations normalized by the mean tidal amplitude (normalized RMS variability (NRMS)) as a metric for stationarity, low-mode M_2 internal tides with NRMS < 0.5 are stationary over 25% of the deep ocean, particularly near the generation regions. The M_2 RMS variability tends to increase with increasing mean amplitude. However, the M_2 NRMS variability tends to decrease with increasing mean amplitude, and regions with strong low-mode internal tides are more stationary. The internal tide beams radiating away from generation regions become less stationary with distance. Similar results are obtained for other tidal constituents with the overall stationarity of the constituent decreasing as the energy in the constituent decreases. Seasonal variations dominate the RMS variability in the Arabian Sea and near-equatorial oceans. Regions of high eddy kinetic energy are regions of higher internal tide nonstationarity.

1. Introduction

There are few eddy-resolving global ocean simulations which contain barotropic tides, internal tides, the general circulation, and mesoscale eddies concurrently, such as the results of 1/12.5° Hybrid Coordinate Ocean Model (HYCOM) forced by realistic atmospheric fluxes and the gravitational attraction of the sun and moon presented here [*Arbic et al.*, 2010]. *Shriver et al.* [2012] find that the global barotropic tides in HYCOM compare well with an altimetry-constrained barotropic tide model (TPXO) [*Egbert et al.*, 1994] and that the model global internal tide amplitudes compare well with an altimetric-based tidal analysis [*Ray and Byrne*, 2010]. The multiyear length of this simulation (2005–2009) and its high horizontal resolution (1/12.5°) allow us to address the question: how stationary are the predicted internal tides as simulated in HYCOM? This question is a keen interest of the satellite altimetry community. Predictable or stationary internal tides could be removed from satellite altimetric sea levels similar to the present-day removal of barotropic tides, which may aid the observation of nontidal submesoscale phenomena in the next generation of wide swath altimeters [*Fu and Ferrari*, 2008; *Chavanne and Klein*, 2010].

One recent attempt to quantify the stationarity of internal tides in the ocean [*Ray and Zaron*, 2011] found that the majority of mode 1 internal tide energy detected by satellite altimetry appeared to be stationary while higher modes were predominantly nonstationary. There were exceptions: east of Brazil even mode 1 was mostly nonstationary. These preliminary results require confirmation and also may be affected by the sampling limitations from orbital mechanics in satellite altimetry. *Ray and Zaron* [2011] use the difference between the wave number spectrum in the expected internal tide wavelengths and a similar spectrum with the point-by-point removal of the 17 year harmonically analyzed tide and a partial correction for aliased nontidal variability as a metric for stationarity.

This paper examines the degree of stationarity in the barotropic and internal tides embedded in a realistic eddy-resolving ocean general circulation model (HYCOM). To investigate the stationarity of the barotropic and internal tides in HYCOM, we estimate tidal amplitudes from 18 overlapping 183 day and 60 contiguous

30 day windows that span the period 2005–2009. The 183 day window size is the minimum necessary to properly resolve the eight tidal constituents presently forced in HYCOM. The 30 day window size only resolves five of the eight tidal constituents but allows an examination of seasonal variability. Variability across the windows for the barotropic and internal tide for the eight tidal constituents is presented and discussed. Possible mechanisms of internal tide nonstationarity including the correlation with the surface eddy kinetic energy (EKE) are discussed.

2. Model

The HYCOM simulation examined in this study has geopotential tidal forcing for M_2, S_2, N_2, and K_2 (the four largest semidiurnal constituents) and for K_1, O_1, P_1, and Q_1 (the four largest diurnal constituents), a scalar self-attraction and loading correction (SAL) [*Ray*, 1998], and a parameterized topographic wave drag [*Arbic et al.*, 2010; updated as described in *Shriver et al.*, 2012] with 32 layers in the vertical and a nominal horizontal resolution of $1/12.5°$ at the equator. For the tides, the model has only two adjustable parameters, the scalar SAL coefficient, and a topographic drag amplification factor. These two parameters are adjusted, using a one-layer barotropic M_2 only version of the model, to minimize the RMS differences between the model M_2 surface elevations and 102 pelagic tide gauges [*Shum et al.*, 1997]. All other parameters are the same as the parameters in the nontidal global model at the same resolution [*Metzger et al.*, 2010].

The model is run interannually over the period of July 2003–December 2010 using 3 h Fleet Numerical Meteorology and Oceanography Center Navy Operational Global Atmospheric Prediction System [*Rosmond et al.*, 2002], atmospheric forcing with wind speeds scaled to be consistent with QuikSCAT observations. No data are assimilated for the tidal simulation. Total sea surface height (SSH) snapshots are saved once per hour for this period. We use the model results from 2005–2009 for this study.

The HYCOM tidal sea surface elevation amplitude and phases are calculated as a complex amplitude using standard harmonic analysis [*Foreman*, 1977] applied to the HYCOM total SSH. We will follow *Shriver et al.* [2012], analyzing the tides along satellite altimeter tracks to facilitate comparison to altimetric tidal estimates such as *Ray and Zaron* [2011]. The HYCOM tidal sea surface elevations are dominated by the barotropic tides, which are estimated from total SSH complex amplitudes using a low-pass spatial filter after interpolating onto the TOPEX/Poseidon/Jason altimeter track grid. The internal tide complex amplitudes are recovered from the total SSH via band-pass spatial filtering to permit wavelengths in the 50–400 km range. The band-pass range spans the length scales of the low-mode internal waves that HYCOM is able to resolve. We note, without showing, that analyses using a steric and nonsteric SSH for baroclinic and barotropic tides have nearly identical results to the band-pass and low-pass spatial filter analyses. All analyses discussed in this paper are limited to locations where the seafloor depth exceeds 1500 m.

3. Results and Discussion

In *Shriver et al.* [2012], global comparisons of barotropic and internal tides generated in our eddy-resolving ocean circulation model are made with tidal estimates obtained from an altimetry-constrained tide model and altimetric sea surface heights, respectively. When compared to a data assimilative model (TPXO7.2), the barotropic tidal errors in HYCOM (M_2 mean square error = 7.48 cm) are comparable to other global nonassimilative shallow water tide models, $\sim$7 cm [*Jayne and St. Laurent*, 2001; *Arbic et al.*, 2004] and $\sim$5 cm for M_2 [*Egbert et al.*, 2004]. The HYCOM internal tide amplitudes, when averaged over internal tide generation regions, compare well (typically within $\sim$20%) to those in along-track altimeter data. Away from the "hot spots," the comparison between the model and altimetric analysis is not as good due, in part, to two problems, errors in the model barotropic tides and overestimation (due to aliasing problems) of the altimetric tides in regions of strong mesoscale eddy activity. The following sections explore the degree of stationarity of the simulated barotropic and internal tides using model data from 2005–2009 and discuss some possible mechanisms responsible for the tidal variability.

3.1. Barotropic Tide

The mean M_2 barotropic tidal amplitude in HYCOM is shown in Figure 1a. The barotropic tidal amplitude is computed from a spatially low-passed tidal analysis of total sea surface height with the mean computed over the 18 overlapping 183 day data windows. The mean amplitude agrees well qualitatively with a one-
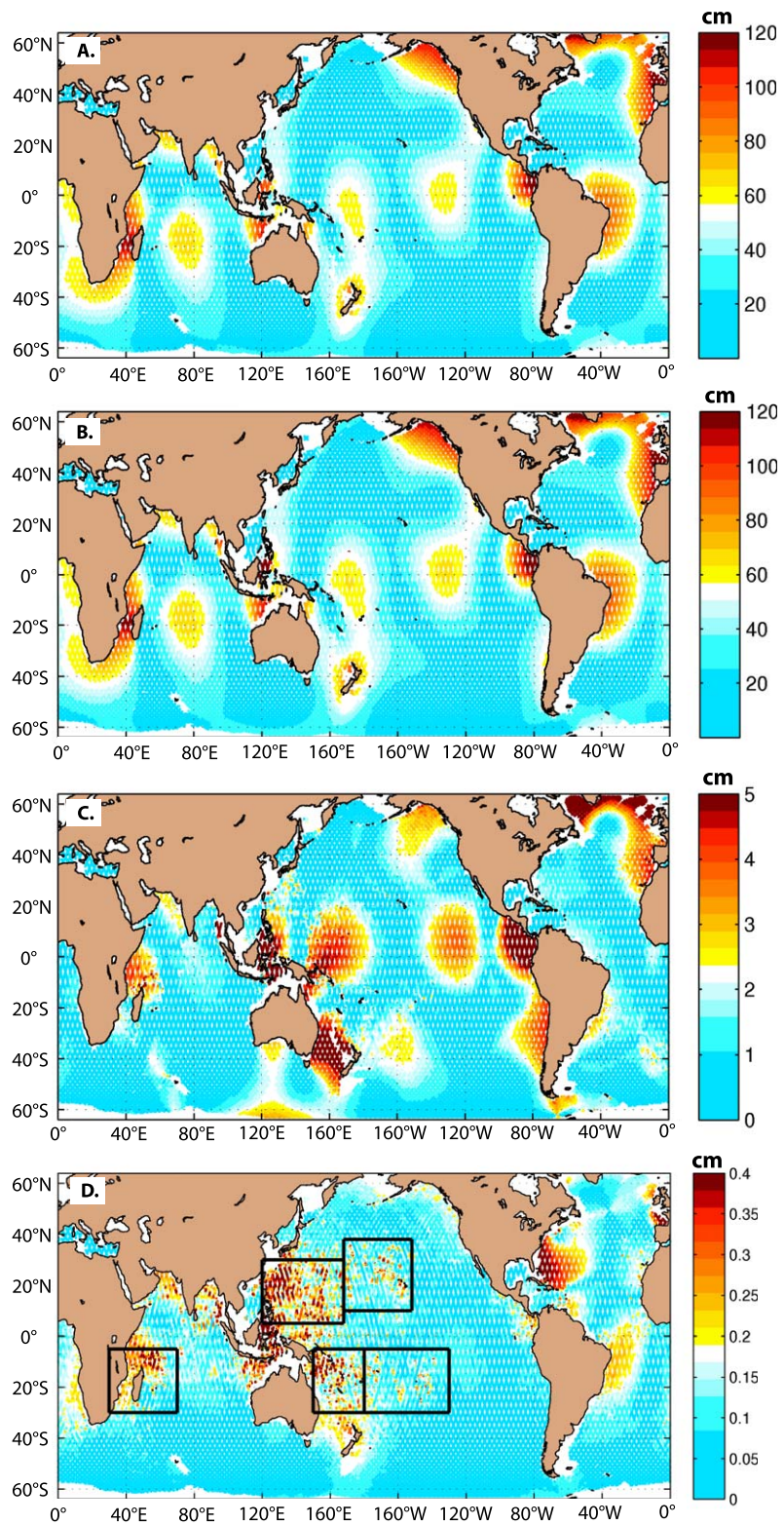
Figure 1. (a) Mean M_2 barotropic tide amplitude from the 32-layer global HYCOM simulation with simultaneous tidal and atmospheric forcing. (b) M_2 barotropic tide amplitude from one-layer HYCOM forced only by tides. (c) The M_2 amplitude difference between Figure 1a and Figure 1b. (d) The barotropic tide amplitude standard deviation computed from the 32-layer global HYCOM simulation with simultaneous tidal and atmospheric forcing. Statistics for Figures 1a, 1b, and 1d were computed over 18 overlapping 183 day data windows as discussed in section 1. The semidiurnal hot spot regions from *Shriver et al.* [2012] are denoted by overlaid black boxes.

layer barotropic, tide-only model (Figure 1b), but there are significant quantitative differences between the mean barotropic tide in the 32-layer baroclinic model and one-layer barotropic model (Figure 1c). Large differences (≥ 5 cm) are found in the tropical Pacific, Tasman Sea, eastern South Pacific, and North Atlantic with smaller amplitude differences (< 5 cm) in areas such as the North Pacific, east of Tanzania, and south of Australia. The differences between the 32-layer and 1-layer tidal amplitudes are not confined to regions where the barotropic tide is large. The RMS variability of the M_2 barotropic tidal amplitude over the 18 overlapping 183 day windows with peak values of ~5 mm (Figure 1d) is much smaller than the mean barotropic tidal amplitudes with peak values >1 m. Areas of relatively large variability, but much smaller than the mean tidal amplitudes, are found in all three major ocean basins, with the lowest variability found in the Antarctic Circumpolar Current region. Again, the areas of large RMS variability are generally not strongly correlated with areas of large barotropic tidal amplitude or large differences between the 32-layer and 1-layer models. Interestingly, the RMS variability of the barotropic tide is large in the regions of large internal tide amplitudes (black boxes in Figures 1d and 2a), but not exclusively as the Atlantic has large RMS variability in regions of low internal tide amplitude as well as low barotropic tide amplitude. Globally, the variability for all barotropic tidal constituents in HYCOM is found to be very small in relation to the mean amplitude, averaging 0.5% or less. The small fractional changes in the barotropic tidal amplitude suggest that the eight barotropic tidal constituents in HYCOM are strongly stationary.

3.2. Internal Tide

How much do the internal tides vary over the period of interest? The mean M_2 internal tidal amplitude over the 18 overlapping 183 day windows from global HYCOM is shown in Figure 2a. The low-mode M_2 internal tide amplitude ranges up to ~4 cm, depending on location. HYCOM has several internal tide generation regions ("hot spots") near Madagascar, Hawaii, east of the Philippines, and the tropical south and southwest Pacific. Internal tides radiating over long distances from the hot spots are also evident, for example, between the Aleutian Islands and the Hawaii hot spots [e.g., *Cummins et al.*, 2001]. Amplitudes fall sharply and are relatively low outside these hot spot regions, although close analysis can reveal internal tide signals even in "quiet" regions such as the southeast Pacific. Figure 2a is essentially identical to Figure 7b from *Shriver et al.* [2012].

For each internal tide constituent, variance of the complex amplitude relative to the mean at a given location can be defined as

$$\sigma^2 = \frac{1}{n} \sum_{j=1}^{n} \left| A_j e^{i\phi_j} - \overline{A} e^{i\overline{\phi}} \right|^2 \tag{1}$$

where n is the number of windows, the overbar denotes an average computed over the n windows, and A and ϕ are the internal tidal amplitude and phase, respectively. Averages were computed using the complex amplitude, where

$$\overline{A} e^{i\overline{\phi}} = \frac{1}{n} \sum_{j=1}^{n} A_j e^{i\phi_j} \tag{2}$$

Following *Shriver et al.* [2012], equation (1) can be rewritten as

$$\sigma^2 = \left(\frac{1}{n} \sum_{j=1}^{n} \left[(A_j - \overline{A})^2 \right] \right) + \left(\frac{1}{n} \sum_{j=1}^{n} \left[2 A_j \overline{A} (1 - \cos(\phi_j - \overline{\phi})) \right] \right) \tag{3}$$

with the first term on the right hand side denoting a contribution to the variance resulting from variations in tidal amplitude-only and the second term from variations in the amplitude-weighted phase. To facilitate comparisons with mean amplitude, the square root of these terms will be considered in subsequent discussion. Note that the amplitude-weighted phase term does not completely represent variability due to changes in phase only, because A_j varies in addition to ϕ_j. To estimate variability due to changes in phase only, A_j can be replaced by $\overline{A}$ in the second term, which we denote as the amplitude-weighted "phase only" variability.
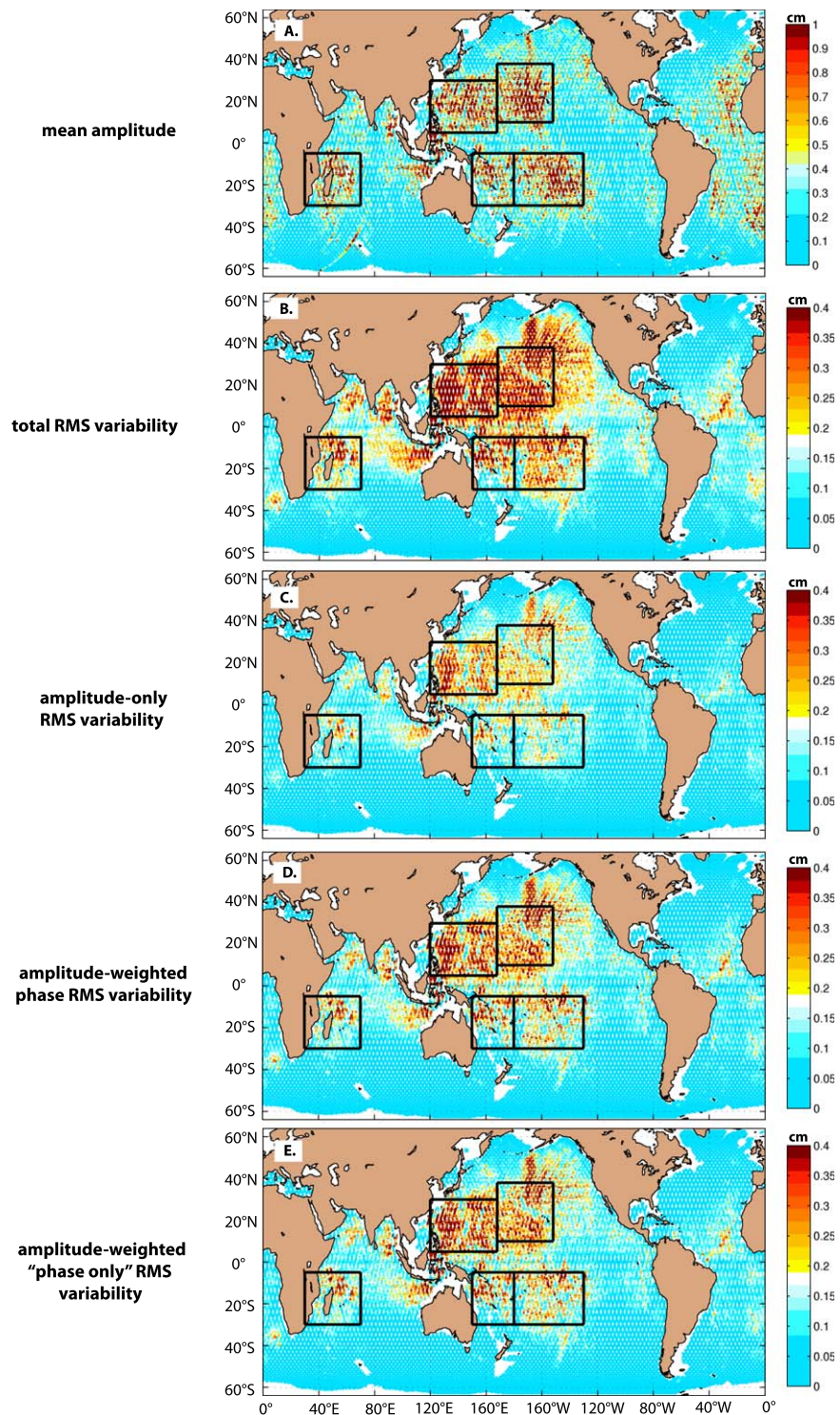
Figure 2. (a) Mean of the M_2 internal tide amplitude from global HYCOM, (b) complex M_2 RMS amplitude variability, computed from equation (1), (c) M_2 RMS amplitude-only variability, (d) M_2 RMS amplitude-weighted phase variability, and (e) M_2 RMS amplitude-weighted "phase only" variability, computed using equation (2). Statistics were computed over the 18 overlapping 183 day data windows. The semi-diurnal hot spot regions from *Shriver et al.* [2012] are indicated by overlaid black boxes.

The RMS variability of the complex M_2 internal tidal amplitude relative to the mean amplitude, as given by (1), is shown in Figure 2b. While the mean internal tide amplitude ranges up to ~4 cm, the RMS variability of the complex amplitude is much smaller, rarely exceeding 4 mm. Areas of larger variability are roughly
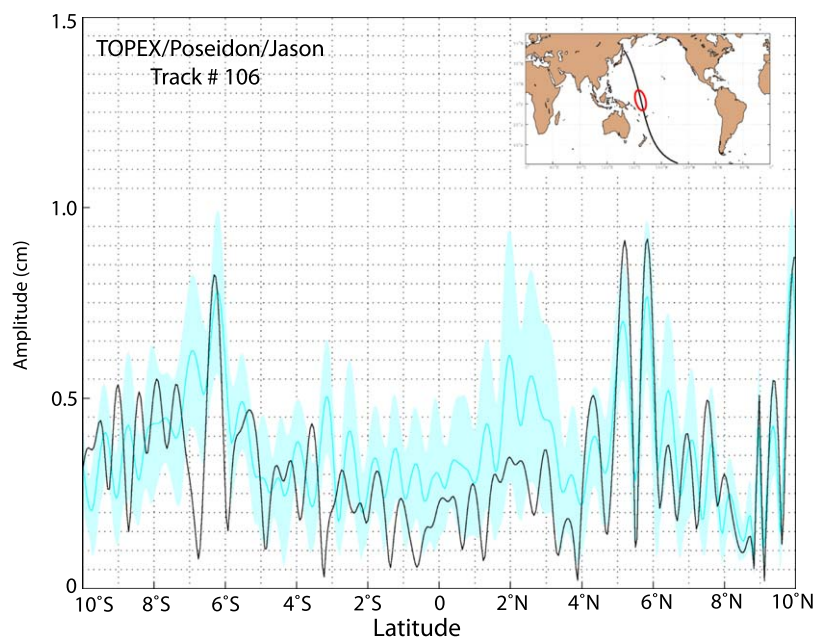
Figure 3. The M_2 internal tide amplitude along an altimeter track (TOPEX/Poseidon/Jason track 106) passing through the western equatorial Pacific at approximately 170°E. Mean M_2 tidal amplitude for the eighteen 183 day HYCOM data windows (solid cyan line) is plotted with ± 1 standard deviation (cyan envelope). For comparison, the M_2 tidal amplitude from a satellite-based tidal analysis is plotted in black. Along this track, the degree of nonstationarity is relatively high with normalized RMS variability ranging from 0.3 to 0.6.

collocated with areas of larger mean amplitude, with a spatial correlation of 0.6. Within the internal tide hot spot regions, the RMS variability is often 3 mm or greater, with large RMS variability in limited areas outside the hot spots such as the eastern tropical Indian Ocean, northeast Pacific Ocean, and the internal tide beams radiating away from the hot spots. Over the entire globe, the amplitude-only variability (Figure 2c) is approximately 40% of the total variability. The amplitude-weighted phase variability (Figure 2d) exhibits qualitatively similar structure, along with slightly higher amplitudes over the Indian and Pacific hot spots. The amplitude-weighted phase variations are almost exclusively due to changes in phase only (illustrated by the minimal differences between the RMS amplitude-weighted phase variability in Figure 2d and the RMS amplitude-weighted "phase only" variability in Figure 2e). RMS variability alone does not indicate the stationarity of the internal tide. To aid interpretation of the RMS variability with respect to stationarity, the RMS variability is normalized by the mean amplitude. The rationale for using normalized RMS (NRMS) variability as a metric for stationarity can be illustrated by examining M_2 internal tide amplitudes plotted along track segments that span areas of high and low normalized RMS variability, respectively.

The M_2 internal tidal amplitude along an altimeter track (TOPEX/Poseidon/Jason track 106) in the western equatorial Pacific at approximately 170°E, which spans an area of high normalized RMS variability, is shown in Figure 3 with the track location shown in the figure inset. The spread of the M_2 tidal amplitudes (depicted by a cyan envelope of ± 1 standard deviation about the mean amplitude) along this transect is often as large as or larger than the mean signal in this area (delineated by a solid cyan line). The black line in the figure is the M_2 tidal amplitude estimated from altimetry along this track [*Ray and Byrne*, 2010]. While the model and altimetric amplitudes do not agree in all details, the overall agreement is good with the average altimetric amplitude at 0.32 cm, while the model average amplitude is 14% higher at 0.37 cm. Along this section of the altimeter track, the mean HYCOM M_2 amplitude ranges from 0.05 to 0.82 cm, the RMS variability from 0.5 to 3.3 mm, and the normalized RMS variability from 0.3 to 0.6. A track crossing the hot spot west of Hawaii at approximately 178°W (TOPEX/Poseidon/Jason track 105), which spans an area of generally high tidal amplitude and low normalized RMS variability, is shown in Figure 4. Along this section of the altimeter track, the mean amplitude ranges from 0.15 to 3.37 cm, the RMS variability from 0.5 to 4.8 mm, and the normalized RMS variability from 0.06 to 0.3. The RMS variability along this section at 178°W is similar in magnitude to the RMS variability along the 170°E section, but the mean amplitudes are ~3–5 times greater with correspondingly smaller normalized RMS variability and greater stationarity. *Ray and Zaron*
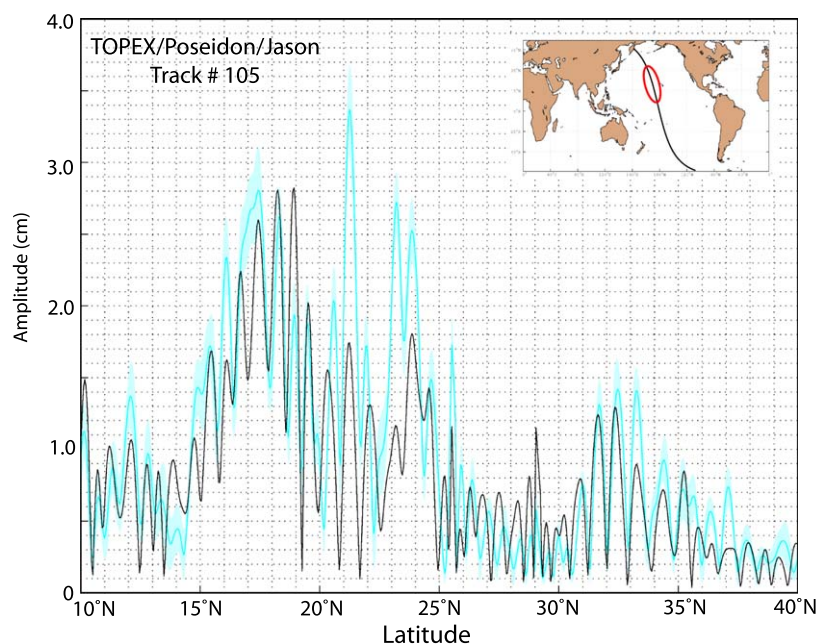
Figure 4. The M_2 internal tide amplitude along an altimeter track (TOPEX/Poseidon/Jason track 105) passing through the Hawaii hot spot at approximately 178°W. Mean M_2 tidal amplitude for the eighteen 183 day HYCOM data windows (solid cyan line) is plotted with ±1 standard deviation (cyan envelope). For comparison, the M_2 tidal amplitude from a satellite-based tidal analysis is plotted in black. In contrast to Figure 3, the internal tide is stationary with normalized RMS variability ranging from 0.06 to 0.3.

[2011] show a similar section through the Hawaii hot spot with RMS variability of 4–6 mm for 2–7 cm mean amplitudes. *Ray and Zaron* [2011] use a different metric for stationarity based upon the along-track wave number spectrum. They find that the RMS variability rarely exceeds 5 mm, consistent with our results. The nonstationary variance estimated by *Ray and Zaron* [2011] rarely exceeds 25% of the mean tidal variance, which is equivalent to our normalized RMS variability of 0.5. Thus, while the largest RMS variability tends to be correlated with the largest mean amplitudes, the largest normalized RMS variability or nonstationarity generally occurs in regions of smaller mean amplitudes.

Is stationarity dependent upon mean amplitude, and if so how strong is the dependence? Using the NRMS variability as a metric for stationarity, two important, practical questions must be addressed. The NRMS variability involves the ratio of the RMS amplitude variability to the mean amplitude. When the mean amplitude is very small and uncertain, then the ratio may be poorly estimated. In the track plots, the RMS amplitude variability had the same range for both tracks, but the mean amplitudes were very different. To investigate the sensitivity of our stationarity metric to tidal amplitude, we consider the histograms of the NRMS amplitude-only and amplitude-weighted phase variability (Figure 5), mean amplitude (Figure 6), and RMS amplitude-only and amplitude-weighted phase variability (Figure 7).

The histograms of the NRMS variability associated with changes in the amplitude-only and with amplitude-weighted phase are shown separately in Figure 5 for each constituent. For all constituents, the amplitude-weighted phase NRMS variability is slightly greater than the amplitude-only NRMS variability. The histograms are plotted with a color coding associated with mean amplitude thresholds. In the figure, histograms using all ocean points are colored cyan. Histograms using ocean points with mean amplitudes greater than 0.5 mm are colored magenta and plotted over the all ocean points histogram. The histograms with larger mean amplitude thresholds are plotted on top of each other with blue representing ocean points with mean amplitude greater than 1 mm, green greater than 1.5 mm, and red greater than 2 mm. Thus, visible cyan-colored histograms represent all points with mean amplitudes smaller than 0.5 mm, magenta represents points with amplitudes between 0.5 mm and 1 mm, blue represents points between 1 m and 1.5 mm, and green represents points between 1.5 and 2 mm. For all constituents, the tails of large nonstationarity are associated with smaller mean amplitudes (cyan and magenta colors in the figure). When we consider all ocean locations, the mean and most probable NRMS variability shift to larger values (increasing
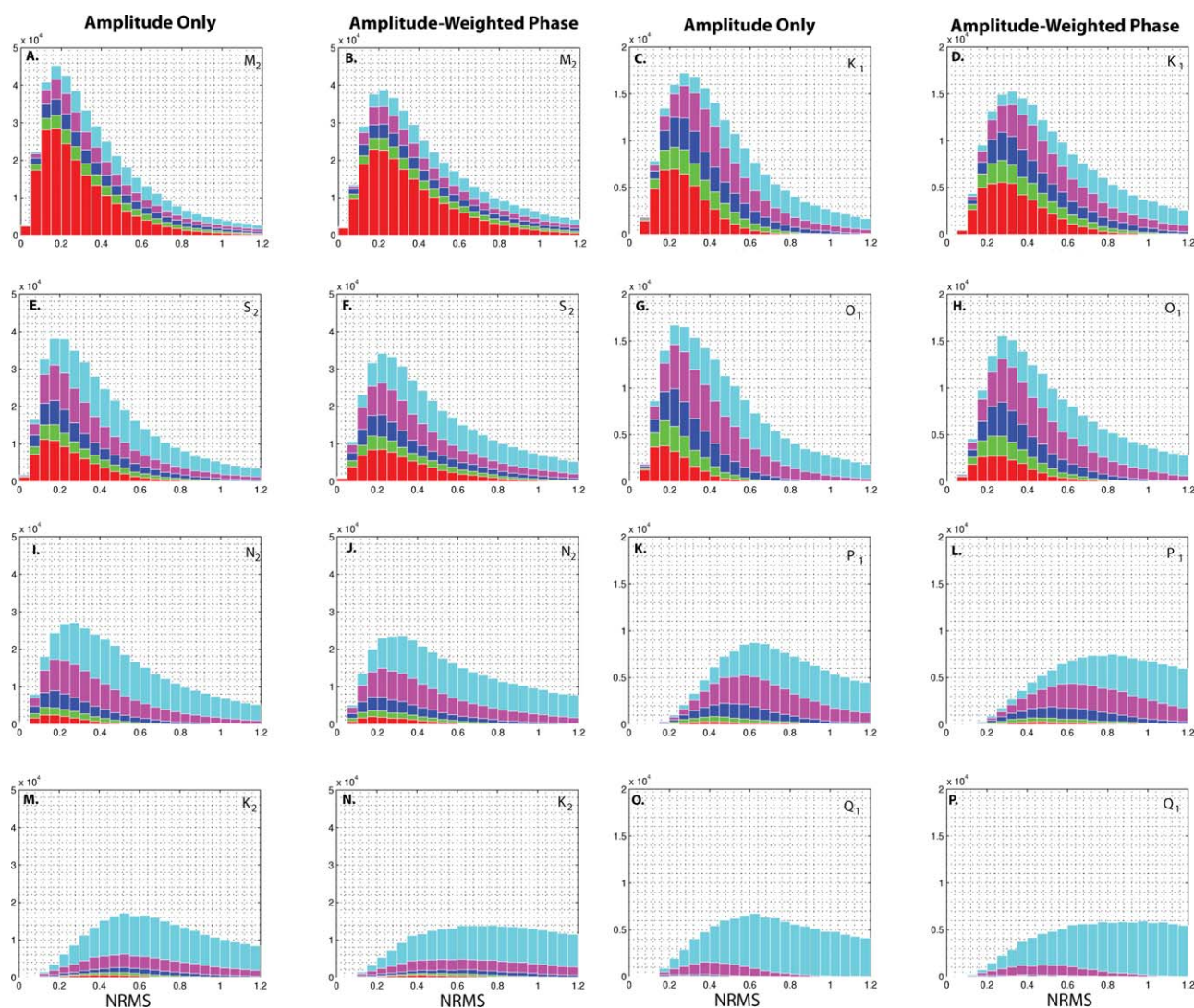
Figure 5. Histograms of normalized RMS (NRMS) variability for the eight tidal constituents in HYCOM. The four semidiurnal constituents are plotted in the first two columns and the four diurnal constituents in the last two columns. NRMS variability resulting from changes in amplitude-only and amplitude-weighted phase for a given constituent are plotted in adjacent columns. To explore the relationship between normalized variability and mean amplitude, we consider changes to their distributions as areas of small amplitude (using thresholds of 0 (cyan), 0.5 mm (magenta), 1 mm (blue), 2 mm (green), and 5 mm (red)) are discarded. Statistics are computed over the 18 overlapping 183 day data windows.

nonstationarity) as the energy of the tidal constituent decreases, with means ranging from 0.63 for M_2 to 2.16 for Q_1 (Table 1). However, if we sort the histograms based upon the mean tidal amplitudes, a different picture emerges. Excluding regions where the mean amplitude is less than 1 mm (cyan and magenta colors), the mean NRMS variability changes very little for the five strongest tidal constituents (0.31–0.39). For two of the weakest tidal constituents, K_2 and P_1, the mean NRMS variability is much larger (0.62 and 0.65, respectively). Additionally, the shape of the histograms changes with the energy in the tidal constituent and with the mean amplitude. The strongest tides, M_2, K_1, S_2, O_1, and N_2, are sharply peaked toward small NRMS, and as thresholds are applied to the histogram the peak moves toward smaller NRMS. For the weaker tides, which are dominated by small mean amplitudes, the peak of the histogram is not as sharply peaked and shifted toward much larger values of the NRMS.

The question arises whether the qualitative change in stationarity with mean amplitude is a real phenomenon or a consequence of the statistical estimation of the tidal amplitudes. If we look at the spatial histograms of the mean tidal amplitudes in Figure 6, we find that even the most energetic tidal constituents have a significant fraction of mean amplitudes smaller than 1 mm, 26% for M_2, 57% for S_2, 53% for K_1, 69% for N_2, and 81% for O_1. For the three weakest constituents, over 88% of the ocean has amplitude weaker
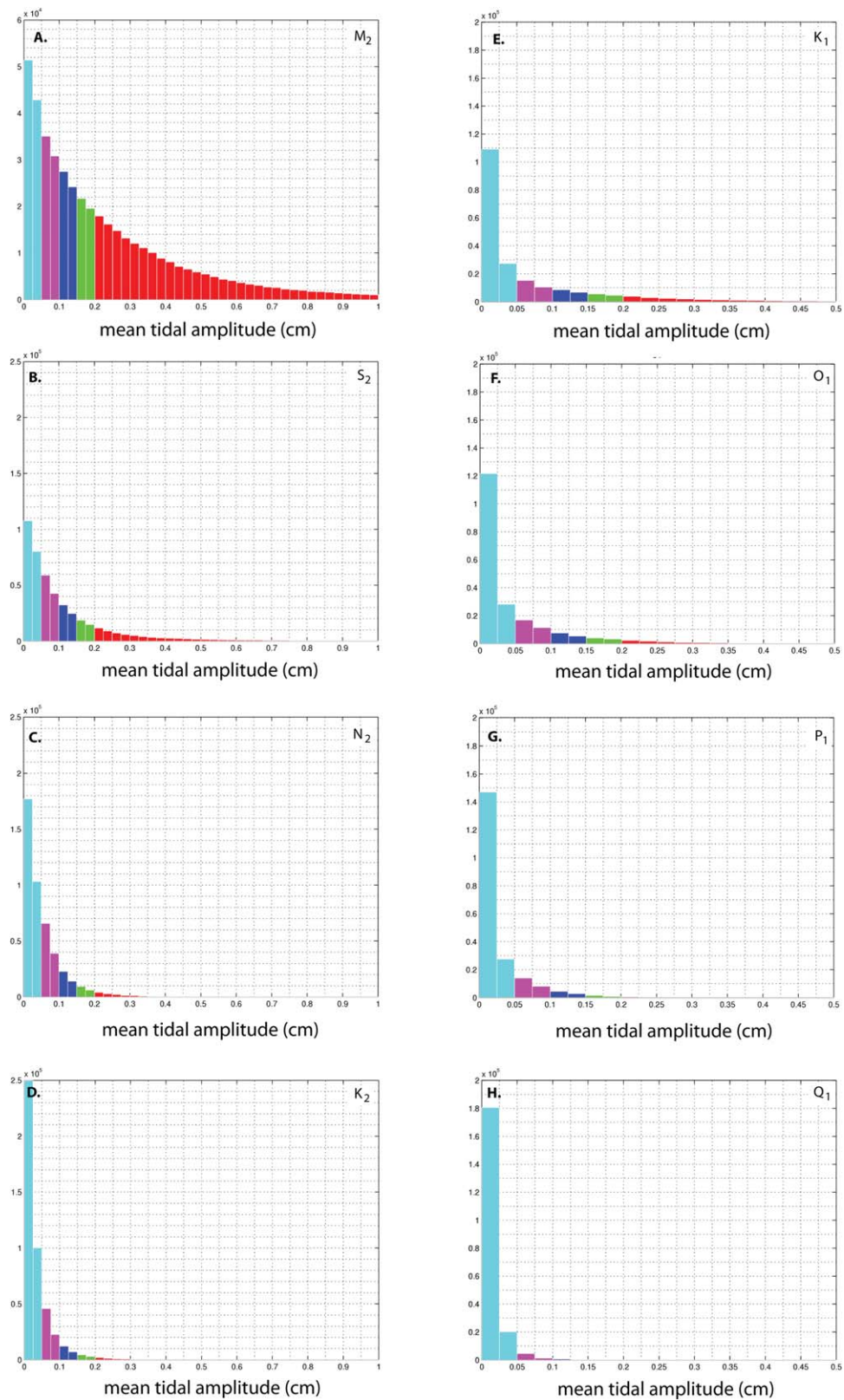
Figure 6. Histograms of mean internal tide amplitude for the eight tidal constituents in HYCOM: (a) M_2, (b) S_2, (c) N_2, (d) K_2, (e) K_1, (f) O_1, (g) P_1, and (h) Q_1. Statistics are computed over the 18 overlapping 183 day data windows and color coded by the thresholds in Figure 5 (0–0.5 mm (cyan), 0.5–1 mm (magenta), 1–1.5 mm (blue), 1.5–2 mm (green), and >2 mm (red)).

Table 1. The Mean Normalized RMS Variability (NRMS) for the Eight Tidal Constituents in HYCOM for All Tidal Amplitudes and for Tidal Amplitudes Greater Than 1 mm (in Parentheses)[a]

Constituent	Mean NRMS
M_2	0.63 (0.39)
K_1	0.78 (0.36)
S_2	0.76 (0.35)
O_1	0.84 (0.31)
N_2	1.16 (0.33)
P_1	1.78 (0.62)
K_2	1.88 (0.65)
Q_1	2.16 (0.36)

[a]Statistics for the semidiurnal constituents are computed globally and for the diurnal constituents are computed over the latitude range $\pm 30°$, which is the range where freely propagating diurnal internal waves exist.

than 1 mm, 88% for K_2, 91% for P_1, and 99% for Q_1. The error in the estimate of the tidal amplitude can be obtained from the signal-to-noise ratio (SNR), which is provided in the standard harmonic analysis package of *Foreman* [1977]. The SNR varies spatially for each constituent, but generally internal tidal amplitudes smaller than 1 mm have a SNR less than 1. We will use 1 mm as the threshold for reliable estimation of the tidal amplitudes. At this 1 mm threshold, a qualitative shift is observed in the shapes of the NRMS histograms. The mean amplitudes of the three weakest constituents are rarely greater than 1 mm.

The histograms of the RMS variability are skewed toward the smallest estimates of variability when all ocean locations are included (cyan histograms in Figure 7). However, for locations with mean tidal amplitudes greater than 1.0 mm, the shape of the histograms changes dramatically with the most probable RMS variability shifting significantly toward larger values (blue, green, and red histograms in Figure 7). Increasing the mean amplitude threshold above 1.0 mm does not change the shape of the histogram significantly, but does shift the most probable RMS variability to higher values (cyan histograms for no threshold, magenta histograms for 0.5 mm threshold, blue histograms for 1 mm threshold, green histograms for 1.5 mm threshold, and red histograms for 2 mm threshold in Figure 7). Changes in the mean and most probable RMS variability with increasing mean amplitude threshold supports the correlation of increasing RMS variability with increasing mean amplitude.

Our metric for stationarity, the normalized RMS variability (Figure 5), has a very different distribution relative to mean amplitude than the un-normalized RMS variability (Figure 7). For the five largest tidal constituents, M_2, S_2, K_1, O_1, and N_2, increasing the mean amplitude threshold does not significantly change the shape of the histogram, but does shift the mean and most probable normalized RMS variability to smaller values. Thus, the stationarity of the internal tide increases with increasing mean tidal amplitude. For the three smallest tidal constituents, K_2, Q_1, and P_1, a very different situation occurs. For these weak constituents, the shapes of the normalized RMS variability distributions are noticeably different, with peaks shifted to higher NRMS values and a much larger fraction of the distribution encompassing values greater than one. For all values of the mean amplitude threshold, there is a tendency for the stationarity to increase with increasing mean amplitude along with a significant shortening of the tail of the distribution encompassing high NRMS values. Because almost all of their values are less than our error threshold, our ability to estimate the SSH tidal amplitude for these weak constituents is marginal. Therefore, little can be said about the stationarity of these weak internal tides, and we will not discuss the weakest constituents, K_2, Q_1, and P_1, in the rest of this paper.

Spatially, the normalized RMS variability (NRMS) of the five significant tidal amplitudes in HYCOM is found to be low in the hot spot regions (denoted by the black boxes in Figures 8), with values generally in the 0.1–0.2 range. For all constituents, the normalized variability due to variations in amplitude and amplitude-weighted phase (left and right columns of Figure 8, respectively) are qualitatively similar, with only small localized differences. For the semidiurnal tides, the normalized RMS variability is larger, exceeding 0.5, in the Pacific Ocean away from the hot spots and in the regions with strong currents and mesoscale eddy activity, such as the Gulf Stream, Kuroshio, Agulhas, Alaska Stream, and Antarctic Circumpolar Current. The mean normalized RMS variability ranges from 0.39 for M_2 to 0.31 for O_1 (Table 1) with similar ranges for the most probable NRMS.

Satellite altimetry provides the only global quantitative observational estimates of the amplitudes of the internal tides [*Ray and Mitchum*, 1996; *Ray and Byrne*, 2010]. *Shriver et al.* [2012] use the along-track altimetric estimates to compare to the model discussed in this paper, and *Ray and Zaron* [2011] discuss the stationarity of the altimetric internal tide amplitudes. However, there are well-known problems recovering the aliased tides from the approximately 10 day sampling of the altimeter, as discussed in *Shriver et al.* [2012, and references therein]. For the circulation model, SSH is sampled hourly which is sufficient to resolve the
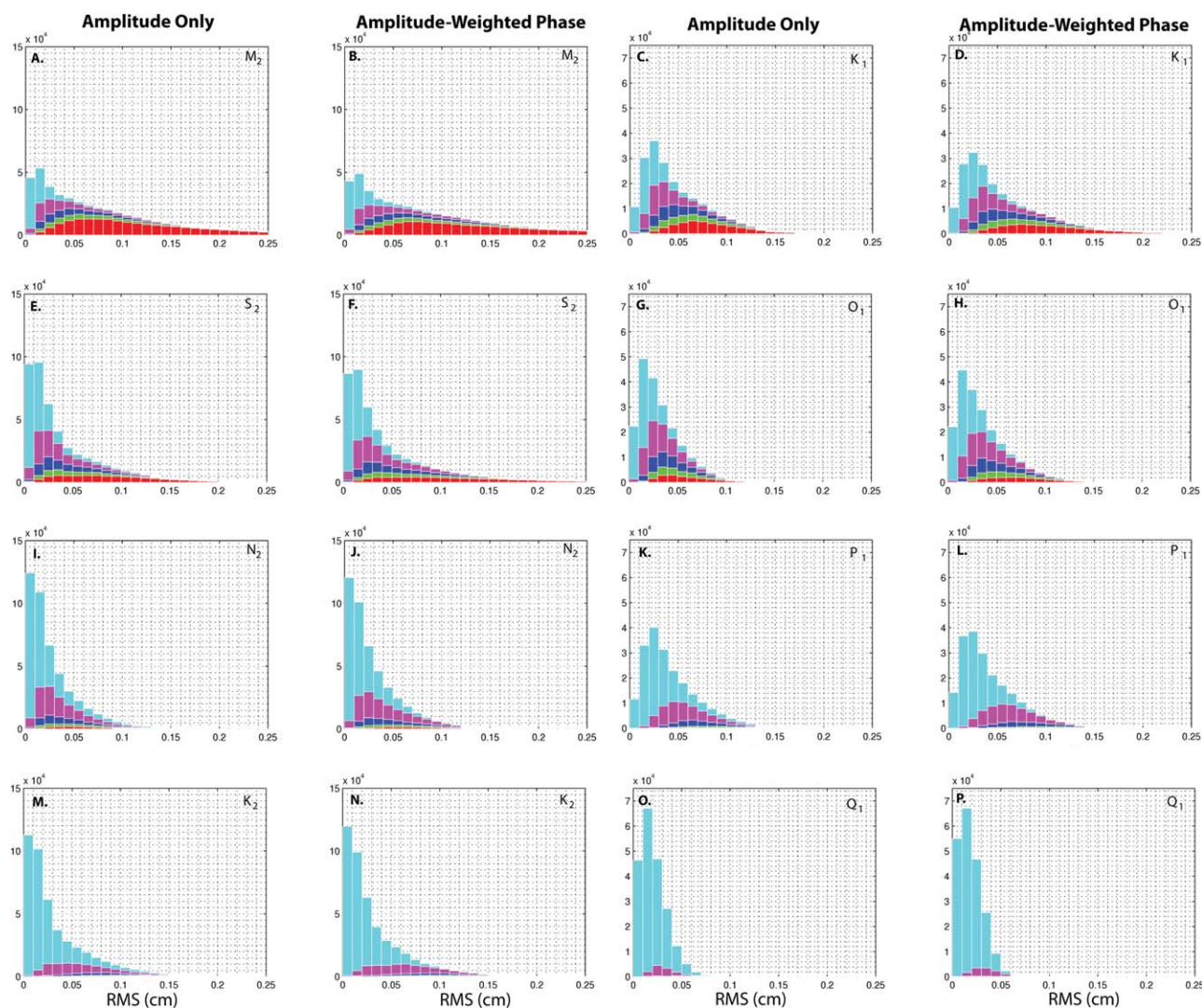
Figure 7. Histograms of RMS variability for the eight tidal constituents in HYCOM. The four semidiurnal constituents are plotted in the first two columns and the four diurnal constituents in the last two columns. RMS variability resulting from changes in amplitude-only and amplitude-weighted phase for a given constituent are plotted in adjacent columns. To explore the relationship between variability and mean amplitude, we consider changes to their distributions as areas of small amplitude (using thresholds of 0 (cyan), 0.5 mm (magenta), 1 mm (blue), 1.5 mm (green), and 2 mm (red)) are discarded. Statistics are computed over the 18 overlapping 183 day data windows.

tidal frequencies and separate the major tidal constituents with the 183 day windows. The question remains whether our analysis is consistent with an altimetric-based tidal analysis [e.g., *Ray and Mitchum*, 1996], where coarse temporal sampling necessitates the recovery of an aliased tidal signal? While we lack a model simulation of sufficient length to reproduce the results of *Ray and Zaron* [2011], analysis of the RMS variability of the M_2 internal tide, using subsampled model data as a proxy for the altimeter data, is presented in Figure 9. The complex tidal amplitude is recovered via a least squares tidal analysis, fitting M_2 and S_2 harmonics to model snapshots of total SSH every 9.92 days (238 h, which is the repeat sampling interval for TOPEX/Poseidon/Jason altimeters) spanning 3 years. A 3 year window is chosen to provide the minimum time series to allow separation of aliased M_2 and S_2 signals. After analysis, the resultant tidal amplitudes are interpolated to TOPEX/Poseidon/Jason track locations. To examine stationarity, three 3 year windows spanning 2005–2007, 2006–2008, and 2007–2009 can be compared to the 18 overlapping 183 day hourly sampled results presented in Figure 2. The mean M_2 tidal amplitude from the simulated altimeter data (Figure 9a) depicts a result similar to that in Figure 2a, but with widespread overestimation of the simulated altimetric tides in regions of strong mesoscale eddy activity such as the Gulf Stream, Kuroshio, Agulhas, Malvinas Confluence, and Antarctic Circumpolar Current [e.g., *Ray and Byrne*, 2010; *Shriver et al.*, 2012]. The
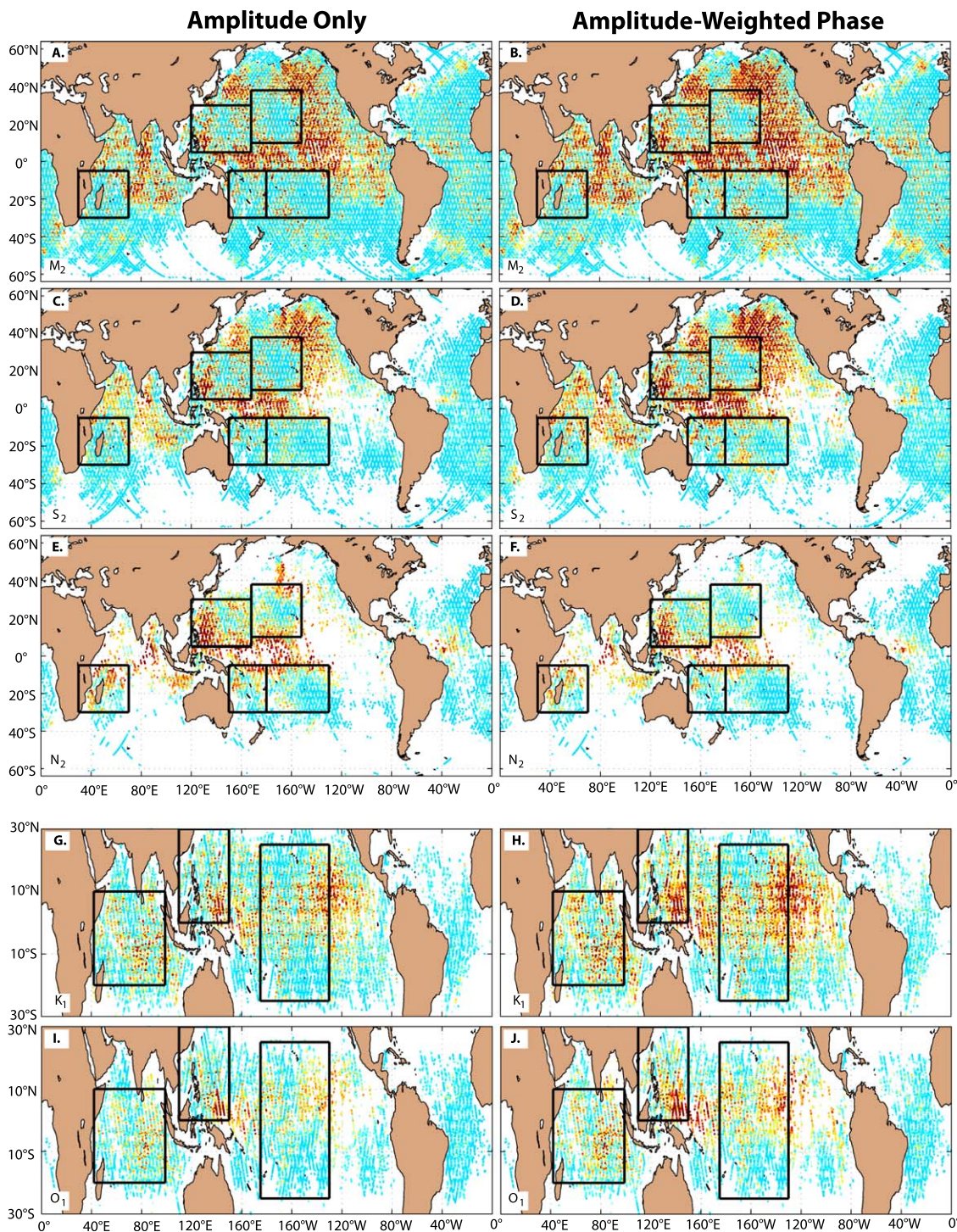
Figure 8. Normalized RMS amplitude-only and amplitude-weighted phase variability over the eighteen 183 day data windows for the five strongest (a–f) semidiurnal and (g–j) diurnal constituents in global HYCOM with regions where mean tidal amplitudes less than 1.0 mm excluded. The RMS amplitude-only variability for each constituent is shown in the left hand column, and the RMS amplitude-weighted phase variability for each constituent is shown in the right hand column. The diurnal and semidiurnal hot spot regions from *Shriver et al.* [2012] are denoted by black boxes. For the diurnal tides in Figures 8g–8j, the latitude range is restricted to the theoretical range where diurnal internal tides exist.

corresponding normalized RMS variability (Figure 9b) is larger than the normalized RMS variability shown in Figure 8a, but the general pattern of stationary internal tides over the hot spot regions with increasing non-stationarity elsewhere is observed. The well-known overestimation of internal tidal amplitudes due to
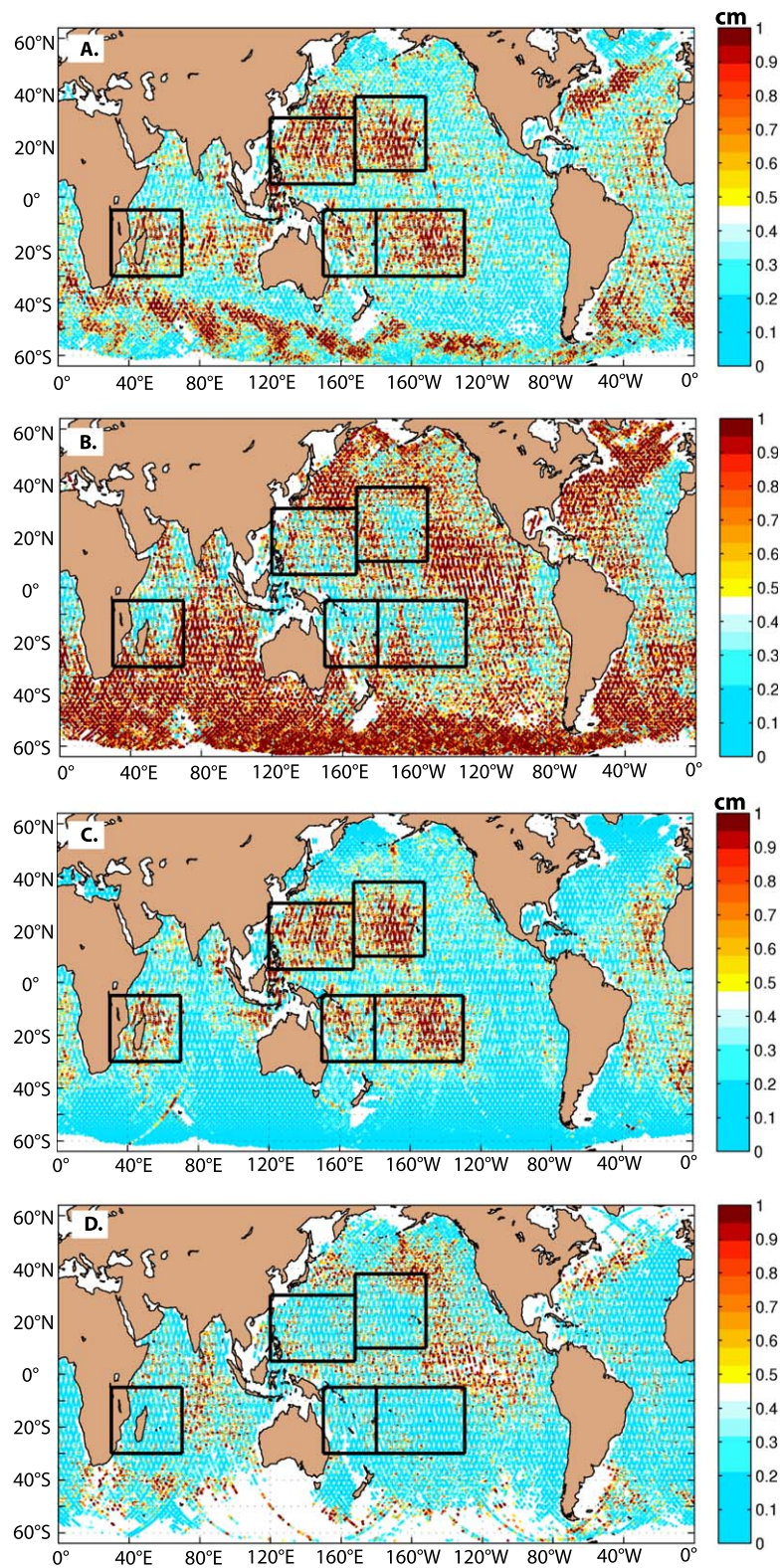
Figure 9. A simulated altimetric-based tidal analysis, using HYCOM SSH subsampled every 9.92 days as a proxy for the altimeter data. The resultant M_2 mean internal tide amplitude (cm) and normalized variability are shown in Figures 9a and 9b. Note mesoscale contamination in regions such as the Kuroshio, Gulf Stream, and Antarctic Circumpolar Current regions. The resultant M_2 mean amplitude (cm) and normalized variability computed after applying a high-pass Butterworth filter to retain tidal periods only are shown in Figures 9c and 9d. In Figure 9d, regions where tidal amplitudes are less than 1.0 mm are excluded.

aliasing of mesoscale variability leads to apparently large nonstationarity in these regions. To remove mesoscale contamination in the simulated altimeter data, we apply a high-pass Butterworth filter with a 2 day cutoff prior to subsampling and subsequent tidal analysis. The resulting mean M_2 tidal amplitude (Figure 9c) and normalized RMS variability (Figure 9d) are found to be qualitatively very similar to that in Figures 2a, 8a, and 8b. With the high-frequency sampling of the model, a "perfect" correction for the mesoscale contamination can be implemented compared to the objective mapping correction of *Ray and Byrne* [2010]. While residual mesoscale contamination may affect the results of *Ray and Zaron* [2011], recovering the tides from aliased height observations does not affect our amplitude and stationarity estimation. The internal tides are stationary near the hot spots with increasing nonstationarity when the tidal amplitudes are low or the mesoscale eddy activity is high.

What is the effect of window size on stationarity? A 183 day window was necessary in order to properly separate all eight tidal constituents in global HYCOM due to the small-frequency difference between (K_2, S_2) and (K_1, P_1) pairs. A problem with this window size is that it could potentially act to damp shorter time scale variability, resulting in lower estimates of NRMS variability. Since we cannot reliably estimate the amplitude of the three weakest constituents (Q_1, P_1, and K_2), we can eliminate them from the tidal analysis, and a window size of approximately 28 days can then be used to properly separate the remaining five constituents.

The M_2 mean amplitude for 60 contiguous 30 day windows is nearly the same as the mean amplitude for the 183 day windows. However, the RMS variability for the 30 day windows more than doubles compared to the 183 day windows. In both the 183 and 30 day windows, the amplitude-weighted phase variability is greater than the amplitude-only variability. However, in the 30 day windows the fraction of the total variability is slightly reduced from 62% to 56% compared to the 183 day windows. The spatial structure of the M_2 NRMS variability obtained from 60 contiguous 30 day windows for both amplitude-only and amplitude-weighted phase (Figures 10a and 10b) is qualitatively similar to the results of the 183 day window analysis presented in Figures 8a and 8b. The shorter data window gives a less stationary tide than the longer data window since the RMS variability more than doubles while the mean stays nearly the same. For the histogram of the NRMS variability (not shown), the peak of the 30 day histogram is shifted to higher NRMS than the 183 day histograms (0.28 compared to 0.18 for amplitude-only and 0.38 compared to 0.2 for amplitude-weighted phase). In addition, the histogram tails, where NRMS greater than 1.0, increase with the shorter data window. Even with the 30 day window, the generation regions are stationary, but the beams of internal tides become less stationary as the beams propagate away from the hot spots. *Zaron and Egbert* [2014] obtained a similar result with their ensemble regional tidal generation and propagation study around Hawaii. As the beams propagate, the amplitude-weighted phase variations represent about 65% of the variance. However, the largest differences between the NRMS variability of the 30 day and 183 day windows are found in the near-equatorial oceans, subtropical Indian Ocean, and regions with strong currents, such as the Kuroshio and Gulf Stream. In these regions, the NRMS amplitude-only variability is slightly greater than the NRMS amplitude-weighted phase variability, which is responsible for the small change in the fraction of amplitude-weighted phase variability for the shorter data window. As discussed in the next section, the increased nonstationarity in these regions is associated with the seasonal cycle, which is not estimated well with the 183 day windows.

3.3. Mechanisms for Variability in the Internal Tides

What are the mechanisms for the variability in the low-mode internal tides simulated in HYCOM? Possible mechanisms include variations due to changes in the ocean stratification, variations in the barotropic tide that generates the internal tide and variations arising from scattering due to mesoscale eddies and strong boundary currents [e.g., *Rainville and Pinkel*, 2006]. Our research strongly suggests the interaction of propagating internal tides through changing stratification and strong currents may be an important mechanism responsible for nonstationarity.

Considering each possible mechanism in turn, the barotropic tide has RMS variability with a similar magnitude to the internal tide RMS variability (Figure 1d versus Figures 2b and 2c). However, the surface expression of the barotropic tide is O(100) larger than its baroclinic counterpart, and the normalized RMS variability of the barotropic tide (not shown) is very small. Because the internal tide is generated by interaction of the barotropic tide with topography in the presence of stratification [*Bell*, 1975], the barotropic variability is too small to explain the internal tide variations.

Seasonal variations in the stratification could be another source of internal tide variability, affecting both the generation and propagation of the internal tide. *Kang et al.* [2002] find 5–10% (∼10 cm) differences
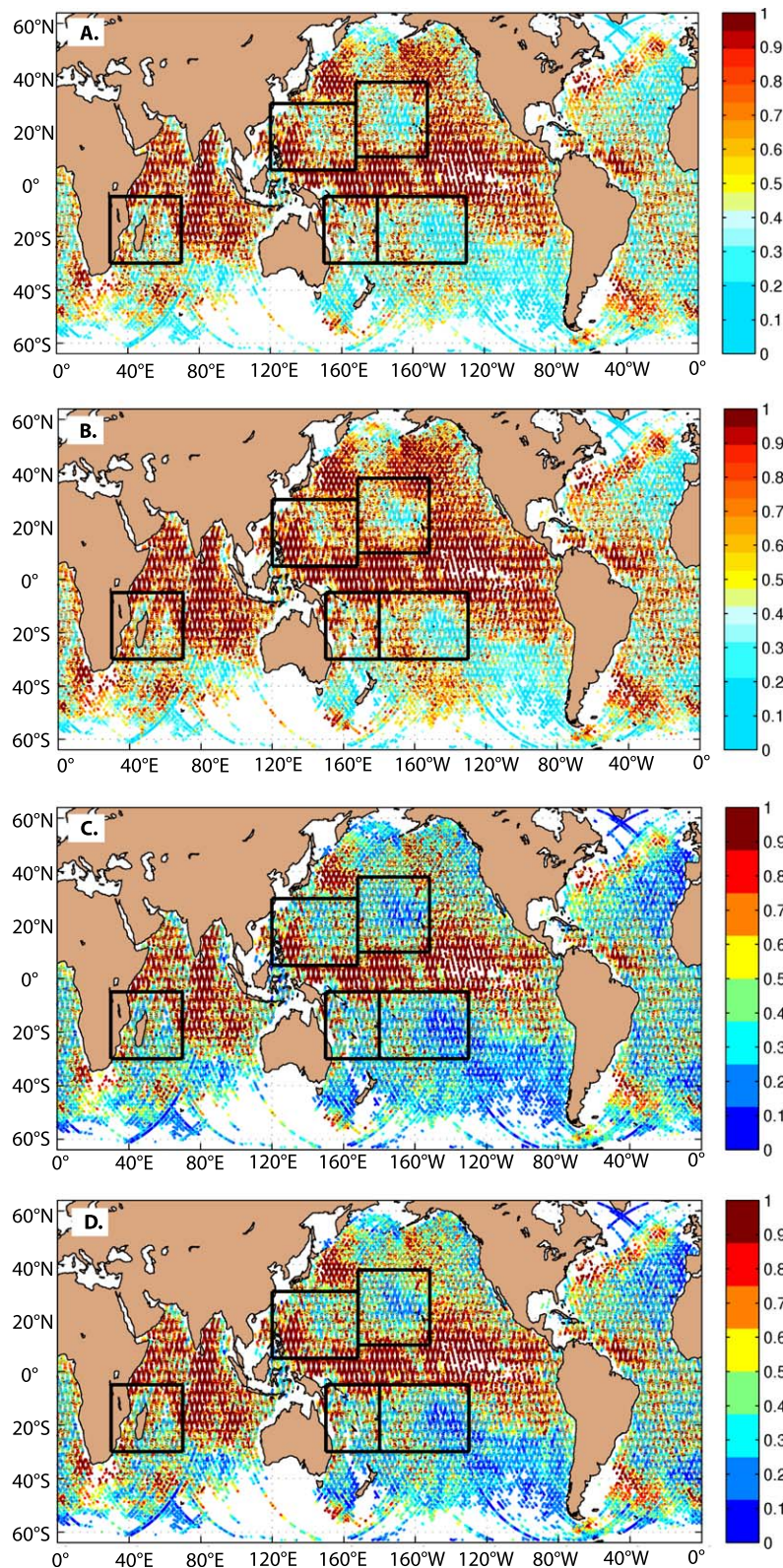
Figure 10. (a) Amplitude-only and (b) amplitude-weighted phase NRMS variability for the M_2 internal tide computed over 60 contiguous 30 day data windows. The changes in the distribution of NRMS variability due to the reduced window size are shown in Figures 10c and 10d. (c) Difference in the M_2 normalized amplitude-only variance between the 30 day windows and 183 day windows (Figures 10a and 8a). (d) Difference in the M_2 normalized amplitude-weighted phase variance between the 30 day windows and 183 day windows (Figures 10b and 8b). The semidiurnal hot spot regions from *Shriver et al.* [2012] are denoted by black boxes. Regions where tidal amplitudes are less than 1.0 mm are excluded.
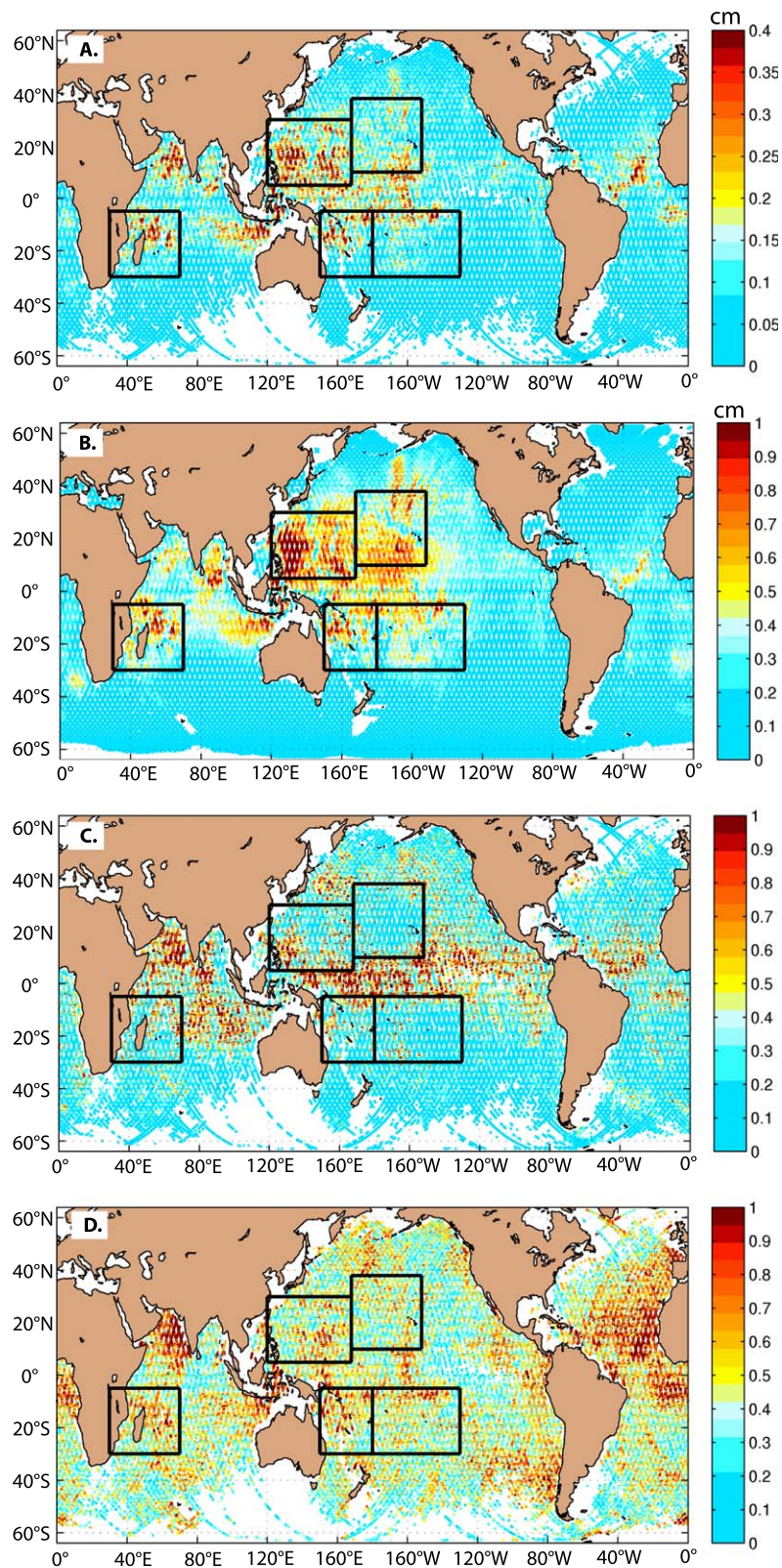
Figure 11. (a) Amplitude of the annual cycle of M_2 internal tide (cm). (b) The RMS M_2 internal tide amplitude variability (cm) over the sixty 30 day windows. (c) The ratio of the amplitude of the annual cycle to the mean amplitude as a measure of the nonstationarity due to seasonal variability, which is greatest in the Arabian Sea and near-equatorial ocean. (d) The ratio of the amplitude of the annual cycle to the RMS amplitude variability over the 30 day windows. Averaged over the ocean 25% of the total RMS variance is seasonal.
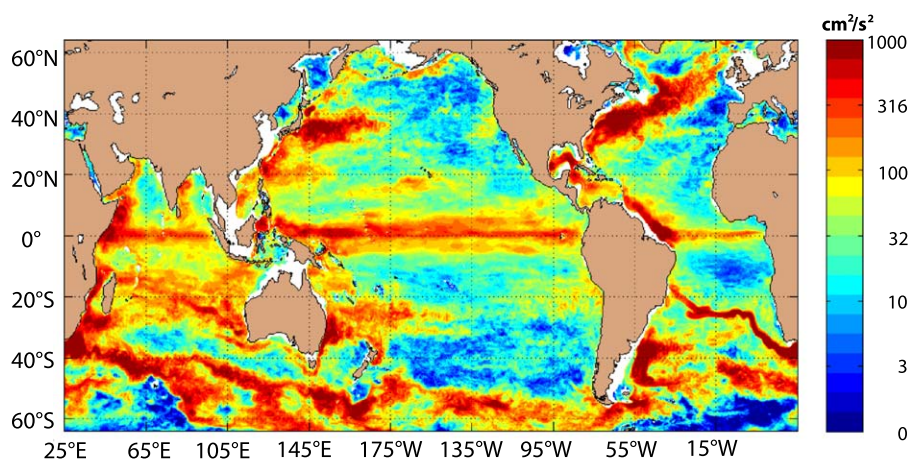
Figure 12. Low-passed eddy kinetic energy (EKE) at 150 m from the 32-layer global HYCOM simulation with concurrent tidal and atmospheric forcing.

between summer and winter coastal barotropic tidal amplitudes in certain regions, where changing stratification leads to changes in the dissipation and barotropic energy flux. While *Ray and Zaron* [2011] find only a few regions with significant summer and winter differences in altimetric internal tidal amplitude, *Müller et al.* [2012] find summer and winter differences of a few mm in model internal tide amplitudes in the hot spots. To estimate the seasonal cycle of the tidal variability in our model, an annual period sinusoid is fit to the time series of amplitudes estimated each month at each location for each constituent. The seasonal cycle of model M_2 internal tide (Figure 11a) is largest in the western tropical Pacific Ocean, the tropical Atlantic Ocean, the Arabian Sea, and north of Madagascar with peak values of ∼4 mm. In the 30 day RMS total variability (Figure 11b), the amplitude and phase variations in the beams radiating away from the generation regions are clearly observed, but these variations are not seasonal. In the regions where the seasonal cycle is the strongest, seasonality strongly contributes to the RMS variability. In Figure 11c, the nonstationarity associated with seasonal variability only is shown. Comparing with Figures 8a and 8b, we observe that the nonstationarity in the Indian Ocean and the near-equatorial Pacific and Atlantic Oceans is dominated by seasonality, while nonstationarity in the eastern Pacific is not seasonal. Over the entire ocean, the variance in the seasonal cycle is about 25% of the variance in the M_2 internal tide (Figure 11d). Our results are consistent with, but more comprehensive than, the altimetric analysis of *Ray and Zaron* [2011] with seasonality dominating the RMS amplitude variability in a limited number of regions.

As noted earlier, the semidiurnal internal tides have a large normalized RMS variability and a greater degree of nonstationarity in regions with strong currents and mesoscale eddy activity. *Rainville and Pinkel* [2006] find significant phase variations for low-mode internal tides propagating through a mesoscale eddy field and significant interactions with meandering western boundary currents. Qualitative correlation between the eddy kinetic energy (EKE) in the model at 150 m (Figure 12) and the normalized RMS variability (Figures 8a and 8b) is observed. However, there are regions such as the eastern Pacific Ocean with large normalized RMS variability but low EKE. Eddy activity, present throughout the world ocean, can impact stratification and hence the propagation of internal tides. However, we cannot quantify this mechanism based on these results.

Zaron and Egbert [2014], using a regional tide model with an ensemble of variable background stratification and currents, show that the primary effect of mesoscale eddies is modifying the propagation rather than the generation of the internal tide. They find approximately 20% of the propagating mode 1 internal tide is adiabatically scattered by changes in the wave phase speed, while the propagating mode 2 internal tide is affected by Doppler shifting as well as phase speed changes. The approach of *Zaron and Egbert* [2014] is similar to ours, where they compare the variance of the tidal elevation to the square of the ensemble mean tidal elevation. *Zaron and Egbert* [2014] call the ensemble mean, the coherent tide, and the deviations from the ensemble mean, the incoherent tide. The coherent tide dominates within 250 km of the generation region with incoherence increasing along the propagating beams with distance outside this region. The results of *Zaron and Egbert* [2014] are consistent with our analysis, but a quantitative comparison is not possible.

4. Summary and Conclusions

The stationarity of the internal tides generated in a high-resolution global ocean circulation model is examined using results from years 2005–2009 of a seven and a half year $1/12.5°$ global simulation that resolves barotropic tides, internal tides, and the eddying general circulation. Tidal stationarity was quantified with tidal analyses computed using 18 overlapping 183 day and 60 contiguous 30 day windows that span the period 2005–2009. The 183 day window size is the minimum necessary to properly resolve the eight tidal constituents in HYCOM. The 30 day windows, which resolve five of the eight tidal constituents, are used to investigate seasonal variability. The main metric used to evaluate stationarity is normalized RMS amplitude variations (amplitude standard deviation normalized by the mean amplitude), where large (small) fractional changes in relation to internal tide amplitude suggest nonstationarity (stationarity).

Overall, the RMS variability in the M_2 tidal amplitude is approximately 2 mm or larger over most of the Pacific and Indian Ocean. The RMS variability of the M_2 tidal amplitude can approach the mean amplitude in weaker tidal areas such as the tropical Pacific and eastern Indian Ocean, but it is small in relation to the mean amplitude over the hot spot regions. The spatial distribution of RMS variability is correlated with the mean tidal amplitude, but the normalized RMS variability is inversely correlated with mean tidal amplitude, consistent with increasing stationarity of the internal tide with increasing internal tidal amplitude. Our normalized RMS variability is roughly equivalent to the square root of the variance ratio used by *Ray and Zaron* [2011]. For the five major tidal constituents, M_2, S_2, K_1, O_1, and N_2, the 30 day normalized RMS variability is less than 0.5 (variance ratio of 25%) over 30%–40% of the ocean, while normalized RMS variability is less than 0.7 (variance ratio of 50%) over 45%–55% of the ocean, which is consistent with the conclusion of *Ray and Zaron* [2011] that the low-mode internal tide is mostly stationary. For the three smallest amplitude constituents, K_2, P_1, and Q_1, a different picture emerges with much larger normalized RMS variability suggesting nonstationary internal tides. However, the amplitudes of these weak constituents cannot be reliably estimated. Excluding regions with mean tidal amplitudes less than 1 mm decreases the average RMS amplitude variability, suggesting that the internal tides are more stationary than initially appears.

What are the mechanisms responsible for the nonstationarity of the simulated internal tides in HYCOM? Possible mechanisms include changes in the ocean stratification affecting the propagation of internal tides [e.g., *Zaron and Egbert*, 2014] and scattering by mesoscale eddies and boundary currents [e.g., *Rainville and Pinkel*, 2006]. Our investigation suggests seasonal variation and mesoscale eddy displacement and current impacts on stratification and internal tide propagation are likely mechanisms responsible for this variability. Follow-on research to this work is planned in order to quantify the impact of these mechanisms on internal wave generation and propagation.

References

Arbic, B. K., S. T. Garner, R. W. Hallberg, and H. L. Simmons (2004), The accuracy of surface elevations in forward global barotropic and baroclinic tide models, *Deep Sea Res., Part II*, *51*, 3069–3101.

Arbic, B. K., A. J. Wallcraft, and E. J. Metzger (2010), Concurrent simulation of the eddying general circulation and tides in a global ocean model, *Ocean Modell.*, *32*, 175–187.

Bell, T. H. (1975), Lee waves in stratified flows with simple harmonic time dependence, *J. Fluid Mech.*, *67*, 705–722.

Chavanne, C. P., and P. Klein (2010), Can oceanic submesoscale processes be observed with satellite altimetry?, *Geophys. Res. Lett.*, *37*, L22602, doi:10.1029/2010GL045057.

Cummins, P. F., J. Y. Cherniawsky, and M. G. G. Foreman (2001), North Pacific internal tides from the Aleutian ridge: Altimeter observations and modeling, *J. Mar. Res.*, *59*, 167–191.

Egbert, G. D., A. F. Bennett, and M. G. G. Foreman (1994), TOPEX/Poseidon tides estimated using a global inverse model, *J. Geophys. Res.*, *99*, 24,821–24,852.

Egbert, G. D., R. D. Ray, and B. G. Bills (2004), Numerical modeling of the global semidiurnal tide in the present day and in the last glacial maximum, *J. Geophys. Res.*, *109*, C03003, doi:10.1029/2003JC001973.

Foreman, M. G. G. (1977), Manual for tidal heights analysis and prediction, *Pacific Mar. Sci. Rep. 77-10*, 66 pp, Inst. of Ocean Sci., Patricia Bay, North Saanich, British Columbia, Canada.

Fu, L.-L., and R. Ferrari (2008), Observing oceanic submesoscale processes from space, *Eos Trans. AGU*, *89*(48), 488, doi:10.1029/2008EO480003.

Jayne, S. R., and L. C. St. Laurent (2001), Parameterizing tidal dissipation over rough topography, *Geophys. Res. Lett.*, *28*, 811–814.

Kang, S. K., M. G. G. Foreman, H.-J. Lie, J.-H. Lee, J. Y. Cherniawasky, and K.-D. Yum (2002), Two-layer tidal modelling of the Yellow and East China Seas with application to seasonal variability of the M_2 tide, *J. Geophys. Res.*, *107*, 3020, doi:10.1029/2001JC000838.

Metzger, E. J., H. E. Hurlburt, X. Xu, J. F. Shriver, A. L. Gordon, J. Sprintall, R. D. Susanto, and H. M. van Aken (2010), Simulated and observed circulation in the Indonesian Seas: $1/12°$ global HYCOM and the INSTANT observations, *Dyn. Atmos. Oceans*, *50*, 275–300, doi:10.1016/j.dynatmoce.2010.04.002.

Müller, M., J. Y. Cherniawsky, M. G. G. Foreman, and J.-S. von Storch (2012), Global M_2 internal tide and its seasonal variability from high resolution ocean circulation and tide modelling, *Geophys. Res. Lett.*, *39*, L19607, doi:10.1029/2012GL053320.

Rainville, L., and R. Pinkel (2006), Propagation of low-mode internal waves through the ocean, *J. Phys. Oceanogr.*, *36*(6), 1220–1237.

Ray, R. D. (1998), Ocean self-attraction and loading in numerical tidal models, *Mar. Geod.*, *21*, 181–192.

Ray, R. D., and D. A. Byrne (2010), Bottom pressure tides along a line in the southeast Atlantic Ocean and comparisons with satellite altimetry, *Ocean Dyn.*, *60*, 1167–1176.

Ray, R. D., and G. T. Mitchum (1996), Surface manifestation of internal tides generated near Hawaii, *Geophys. Res. Lett.*, *23*, 2101–2104.

Ray, R. D., and E. D. Zaron (2011), Non-stationary internal tides observed with satellite altimetry, *Geophys. Res. Lett.*, *38*, L17609, doi:10.1029/2011GL048617.

Rosmond, T. E., J. Teixeira, M. Peng, T. F. Hogan, and R. Pauley (2002), Navy operational global atmospheric prediction system (NOGAPS): Forcing for ocean models, *Oceanography*, *15*, 99–108.

Shriver, J. F., B. K. Arbic, J. G. Richman, R. D. Ray, E. J. Metzger, A. J. Wallcraft, and P. G. Timko (2012), An evaluation of the barotropic and internal tides in a high-resolution global ocean circulation model, *J. Geophys. Res.*, *117*, C10024, doi:10.1029/2012JC008170.

Shum, C.-K., et al. (1997), Accuracy assessment of recent ocean tide models, *J. Geophys. Res.*, *102*, 25,173–25,194.

Zaron, E. D., and G. D. Egbert (2014), Time-variable refraction of the internal tide at the Hawaiian Ridge, *J. Phys. Oceanogr.*, *44*(2), 538–557, doi:10.1175/JPO-D-12-0238.1.